

# Recent Development of Indoor Organic Photovoltaics

Muheeb Ahmad Alkhalayfeh,\* Azlan Abdul Aziz,\* Mohd Zamir Pakhuruddin, Khadijah Mohammedsaleh M. Katubi, and Neda Ahmadi

Solar energy technologies provide solutions for the effective exploitation of internet of things (IoT)-based applications such as smart devices. Organic photovoltaics (OPVs) fabricated from  $\pi$ -conjugated carbon-based semiconductors have shown great potential for indoor applications based on exceptional properties that include small current leakage under dim lighting, large absorption coefficient, and low-cost solution processes. However, organic cells need additional enhancements, such as improving their dim light absorption and exploiting suitable bandgap materials, to make the best use of indoor lighting photons. This article highlights the crucial role of the theoretical basis of photovoltaics and reviews the effect of active layer thickness. Furthermore, the crucial advancements in material design for indoor OPVs are highlighted herein. Lastly, the contribution of plasmonic effect of metallic nanoparticles (MNPs) to improve the performance of OPVs is elaborated, which could contribute to raising the efficiency of energy conversion and reaching production scale criteria.

## 1. Introduction

The development of indoor electronic gadgets for internet of things (IoT) has inspired the fabrication of photovoltaic (PV) devices capable of efficient conversion of indoor light into electricity. These miniature electronic devices can be operated using a small quantity of energy (i.e., batteries). However, the duration of batteries is limited, which restricts their use. Over the years, in-depth studies have been carried out on organic photovoltaic (OPV) devices, simultaneously with their inorganic equivalents to determine their potential use as viable power sources for the manufacture of solar-based devices such as transparent windows and indoor devices.<sup>[1–3]</sup> Their exceptional performance and portable use can be attributed to their cost-effectiveness, low

weight, transparency, flexibility, and energy-level tunability.<sup>[4–6]</sup> However, the photovoltaic performance of OPVs when illuminated with sunlight is lower compared to crystalline silicon (c-Si) for a number of reasons that include 1) high sensitivity to the intensity of sunlight, 2) restricted absorption of the incident light because of the active layer thickness, which is typically around 200 nm, 3) low internal quantum efficiency (IQE) due to short exciton diffusion length and low carrier mobility, 4) poor exciton diffusion lengths of the carriers, which is attributable to limited hopping transport, and 5) instability.<sup>[7]</sup>

Nonetheless, numerous prior researches reported that OPVs have a more efficient light conversion performance than other inorganic technologies owing to their small current leakages under low lighting

condition.<sup>[8–10]</sup> Furthermore, as related to indoor power generation, OPVs have the benefits of higher  $V_{oc}$  and more compatible absorption spectrum compared to c-Si solar cells.<sup>[11]</sup> Thus far, power conversion efficiencies (PCEs) of over 31% have been attained for indoor organic photovoltaic (IOPV) cells under light-emitting diodes (LEDs) lamp with intensity ranging between 100 and 1700 lx<sup>[12]</sup> and reached approximately 17% under 1 sun illumination.<sup>[13,14]</sup> This enables a power output that exceeds  $30 \mu\text{W cm}^{-2}$ , under indoor illumination (500 lx), which is sufficient for communication gadgets and sensors. Conversely, PCEs of about 20% have been achieved for c-Si under LED illumination.<sup>[15]</sup>

Based on these advantages, IOPV is a preferred power generation or supplement source capable of harvesting energy from photons of indoor light (**Figure 1**), which is crucial in the near future. Moreover, the annual global demand for indoor photovoltaic (IPV) is projected to surpass \$850 million by 2023, with the potential to stay significant in the years ahead.<sup>[16]</sup>

Several researches have been conducted on IPVs. The artificial indoor lighting sources comprise compact fluorescent lamps (CFLs), LED lamps, incandescent light bulbs, and halogen lamps. Indoor illumination has a brightness of 200–1000 lx, which is 100–500 times lower than the 1 sun illumination. The emission spectrum of indoor lighting sources, compared to the 1 sun condition, is in the visible band, ranging from 380 to 760 nm.<sup>[17,18]</sup> The emission spectrum and irradiance intensities of indoor illumination sources are different from the AM1.5 G light source as shown in **Figure 2**. The variation or specific spectrum range depends on the particular light source, intensity, and color rendering. LEDs have some advantages when compared to CFLs and

M. A. Alkhalayfeh, A. Abdul Aziz, M. Z. Pakhuruddin  
School of Physics  
Universiti Sains Malaysia  
11800 USM, Pulau Pinang 11800, Malaysia  
E-mail: muheebphy@yahoo.com; lan@usm.my

K. M. M. Katubi  
Chemistry Department, College of Science  
Princess Nourah bint Abdulrahman University  
Riyadh 11671, Saudi Arabia

N. Ahmadi  
Department of Basic Sciences  
Islamic Azad University  
Garmsar Branch, Garmesar 1584743311, Iran

 The ORCID identification number(s) for the author(s) of this article can be found under <https://doi.org/10.1002/pssa.202100639>.

DOI: 10.1002/pssa.202100639

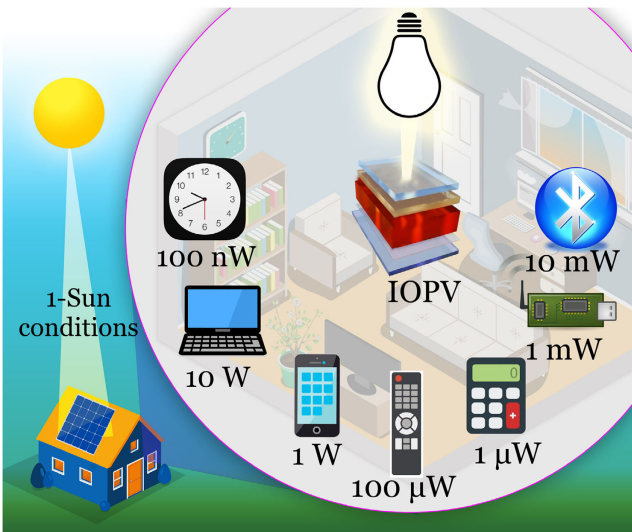


**Figure 1.** Small electrical devices can be charged under dim lighting condition using IOPVs.

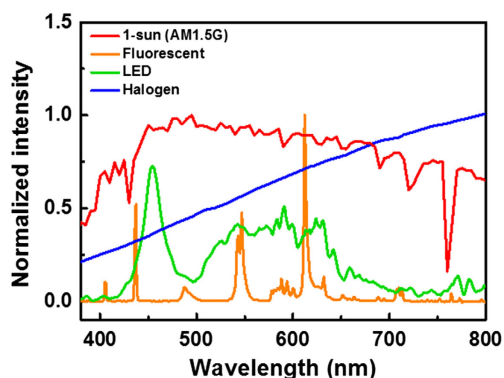


**Figure 2.** Emission spectrum for the AM1.5G light source and indoor light sources (FL lamp, LED lamp, and halogen lamps). Adapted with permission.<sup>[29]</sup> Copyright 2019, Elsevier.

incandescent light bulbs. LED technology has products with luminous efficiency similar to the more efficient light sources on the market and it is expected to dominate indoor light sources in IoT applications.<sup>[19]</sup> According to the studies, the PCE limit of OPVs when using FLs may approach 50%, whereas it can reach 60% when using LED lighting sources.<sup>[20–22]</sup> On the other hand, the bandgap of photoactive materials of OPV is one of the most important factors affecting PCE. However, most wide-bandgap OPVs' active layers have a substantial absorption in the visible wavelength range of 380–760 nm, which matches the emission spectra of indoor illumination sources (i.e., LED and FL). Therefore, the optimum bandgap for IOPVs is between 1.8 and 2.0 eV.<sup>[11,23,24]</sup> In contrast, under AM1.5G condition, wide-bandgap materials are not suited for achieving high PCEs.<sup>[25,26]</sup>

To optimize the generation of indoor power, diverse approaches have to be considered during the design of indoor light harvesting resources and device configurations that differ from the currently available solar cells. Several prior studies

examined the various photovoltaic behaviors of OPVs under 1 sun condition and different ambient lighting conditions and environments. Structural and molecular optimizations of the devices to optimize the ambient light harvesting were discussed. One of the several issues hindering the PCEs of IPVs is the much narrower emission spectra of indoor lighting sources than the conventional solar spectrum. In addition, indoor lighting sources have considerably lesser irradiance intensities (about 1000 times lower) as compared to that of the outdoor 1 sun condition, which predictably leads to the generation of drastically lower photocurrent.<sup>[27,28]</sup> Therefore, there is the utmost need to optimize the photocurrent being generated by IPVs. This article provides a detailed review of the basic concepts of IOPVs with regard to their light-trapping mechanisms, principles, and approaches to achieve high PCEs in indoor environments, a synopsis of the current advancements in the field of IOPVs, as well as the major constraints encumbering the attainment of high PCEs.

## 2. Theory of Photovoltaic Cells

Improved efficiency of photovoltaic cells via spectrum matching of the active material, minimization of voltage loss to the extent that is feasible, and prevention of trap-assisted recombination of excitons is a critical rule to enhance electrical properties of the devices. Thus, it would be useful to elucidate the interaction of the fundamental parameters with incident light and hypothetical calculations for photovoltaics before detailing the application of OPVs for indoor devices. In the case of outdoor applications, power density is utilized to denote the intensity of incident light. On the other hand, the indoor light intensity is generally expressed in terms of the intensity of its illumination ( $E_V$ , lx) as shown by Equation (1).  $E_V$  (unit: lx) is a derivative of the emission spectrum obtained using a spectrometer and  $V(\lambda)$ . The illumination for indoor settings is usually within the intensity range of 100–1000 lx, which signifies the illumination prerequisite for diverse indoor locations. For instance, 200, 500, and 1000 lx are recommended for living rooms and hallways or passages; offices and classrooms; and superstores and theatres, respectively. These illumination intensities only signify  $\approx 0.1\text{--}1\%$  of the benchmark sunlight intensity. More specifically, the illumination intensity of indoor condition is two to three orders of magnitude below 1 sun condition. The intensity of sunlight is about  $10^5$  lx.<sup>[30–34]</sup> Because of this considerable difference in illumination, the carrier density in IOPV cell is drastically less than that for outdoor cells, leading to recombination processes and different charge transport, thus resulting in a predictable decline in  $V_{oc}$ . Nonetheless, this decrease or loss of  $V_{oc}$  has to be minimized, which can be achieved by deciphering the theoretical calculations of the  $V_{oc}$ .  $V_{oc}$  is described based on the electron and hole quasi-Fermi levels of semiconductors. In Equation (2),  $E_{Fn}$  shifts up and  $E_{Fp}$  shifts down by decreasing light intensity, which accounts for the reduction of  $V_{oc}$  due to the decline in illuminances,<sup>[35]</sup> as shown in Figure 3. Furthermore, the  $V_{oc}$  depends on the photocurrent as articulated in Equation (3) which explains that the minimization of the  $J_0$  can contribute to the maximization of  $V_{oc}$ . Specifically, the carrier density is very low under dim lighting, affecting the  $V_{oc}$ .<sup>[12,36]</sup>

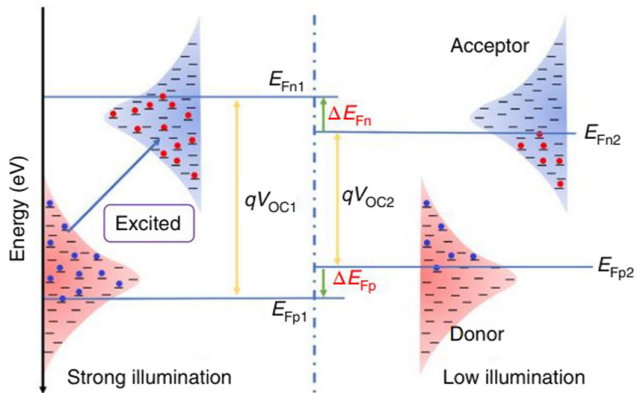


**Figure 3.** Schematic diagram of the density of states under high and low illumination intensity in the donor and acceptor materials. Adapted with permission.<sup>[42]</sup> Copyright 2019, Springer Nature.

In addition, the loss of  $V_{oc}$  under dim lighting is expressed by Equation (4).

Under the 1 sun condition (AM1.5), the energy loss ( $E_{loss}$ ) stems from free carrier derived losses and the charge transfer losses. The recorded  $E_{loss}$  for the most efficient organic solar cells (OSCs) is about (or greater than) 0.6 V under AM1.5.<sup>[37,38]</sup>  $E_{loss}$  is the product of optical bandgap of the acceptor, measured as  $qV_{oc}$ , as expressed in Equation (5). Conversely, under dim or weak illumination, the carrier density significantly decreases, and trap-assisted recombination considerably hinders the efficiency of electrodes in the accumulation of charge carriers.<sup>[39]</sup> Consequently, the trapping can affect the fill factor (FF) because the FF has a proportional relationship with the  $V_{oc}$  that differs depending on illumination (see Equation 6).<sup>[40]</sup>

More specifically, an additional increase in light intensity will lead to a significant increase in  $r_s$  (where  $r_s = R_s/R_{ch}$  and  $R_{ch} = V_{oc}/(J_{sc}A)$ , resulting in lowering of FF values and dominance of recombination of excitons in OPV cells.<sup>[23]</sup> On the contrary, the recombination of excitons decreases as light intensity declines, which leads to an increase in FF. However, in the case of a significant decrease in light intensity, the decline in carrier

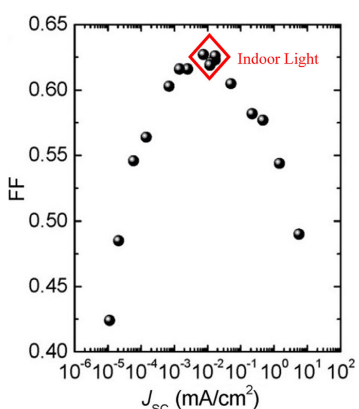


**Figure 4.** Chart of FF on a semilogarithmic scale under differing light irradiance. Adapted with permission.<sup>[43]</sup> Copyright 2014, Royal Society of Chemistry.

density increases the proportion of trap-assisted recombination of excitons, resulting in a decrease in FF. **Figure 4** illustrates the considerably higher FF of IOPVs devices compared to those under the 1 sun condition, as reported in prior works. Furthermore, the potential effects of  $R_s$  and  $R_{sh}$  on the PCE of OPV devices for outdoor and indoor applications vary.  $R_s$  largely stems from the resistance of the active layers, interfacial layers, and transparent electrodes, while  $R_{sh}$  is associated with leakage currents. It can be noted from the Shockley Equation (7) that it is not necessary to have a large  $R_{sh}$  to maintain high  $V_{oc}$ , but also a reduction of  $R_s/R_{sh}$  in order to achieve high  $J_{sc}$  and PCE.<sup>[34,41]</sup> Lastly, the output power based on a photovoltaic cell depends on the  $J_{sc}$  and  $V_{oc}$  of the device, as well as the FF at a specified incident power ( $P_{in}$ ) as shown by the formula:  $PCE = P_{out}/P_{in} \times 100$  where  $P_{out} = V_{oc} \times J_{sc} \times FF$  and  $P_{in}$  should be precisely calculated.

$$E_v = K_m \int_0^\infty E_\lambda(\lambda) V(\lambda) d\lambda \quad (1)$$

where the coefficient  $K_m = 683 \text{ lm W}^{-1}$ ,  $V(\lambda)$  according to commission international de l'Eclairage (CIE) luminous efficiency functions for human eye, and  $E_\lambda$  is the emission spectrum ( $\text{W cm}^2 \text{ nm}^{-1}$ ) $^{-1}$ .

$$V_{oc} = 1/q(E_{Fn} - E_{Fp}) \quad (2)$$

where  $q$  denotes the elementary charge,  $E_{Fn}$  is the electron quasi-Fermi levels, and  $E_{Fp}$  indicates hole quasi-Fermi levels.

$$V_{oc} \approx \frac{n k T}{q} \ln \left( \frac{J_{ph}}{J_0} + 1 \right) \quad (3)$$

where  $n$ ,  $T$ ,  $k$ ,  $J_0$ , and  $J_{ph}$  represent the ideality factor, temperature of the cell, Boltzmann's constant, reverse saturation current density, and photocurrent density (correlates linearly with the light intensity), respectively.

$$\Delta V = \frac{n k T}{q} \ln \frac{I_{ph,sun}}{I_{ph,room}} \quad (4)$$

where  $I_{ph,sun}$  denotes photocurrent under 1 sun illumination and  $I_{ph,room}$  stands for the indoor illuminance condition.

$$E_{loss} = E_g - qV_{oc} \quad (5)$$

where  $E_{loss}$  and  $E_g$  are the energy loss and bandgap, respectively.

$$FF = FF_{sh} = FF_s \left[ 1 - \frac{(V_{oc} + 0.7)FF_s}{V_{oc}r_{sh}} \right] \\ \left( V_{oc} > 10, r_s + \frac{1}{R_{sh}} < 0.4 \right) \quad (6)$$

where  $R_{sh}$  and  $R_s$  are the shunt resistance and series resistance, respectively;  $r_s = R_s/R_{ch}$ , and  $r_{sh} = R_{sh}/R_{ch}$ ;  $R_{ch} = V_{oc}/AJ_{sc}$  (where  $A$  is the photoactive area of the cell).

$$J = \frac{R_{sh}}{R_{sh} + R_s} \left( J_0 \left[ \exp \left( \frac{q(V - JR_s)}{nkT} \right) - 1 \right] + \frac{V}{R_{sh}} \right) - J_{ph} \quad (7)$$

### 3. Effect of the Active Layer Thickness

The PCE of PV cells is dependent on the light absorption capacity of the cell's active layer, the effective dissociation of excitons, and the accretion of charge carriers. Nonetheless, a major limitation that hinders OPVs' performance is the intrinsic trade-off between effective light absorption capacity and accumulation of photogenerated excitons. Here, the thickness of the active layer serves a crucial role. For instance, an active layer thickness of 300–1000 nm results in an increase in absorbed photons' quantity. On the other hand, this thickness leads to an increase in the recombination of excitons that is undesirable, which is the main reason for the low PCE of both organic and polymer solar cells.<sup>[7]</sup> Hence, as the absorption coefficients of OPVs materials are much lower than those of inorganic counterparts, the active layer thicknesses of optimized organic/polymer solar cells are usually small, typically around 200 nm. Therefore, majority of high PCEs were achieved using active layers with a thickness range of 100–200 nm.<sup>[44–49]</sup> Remarkably, the active layer thickness has variable effects on the behaviors of IOPVs devices and outdoor devices such as polymer solar cells (PSCs)/OSCs under 1 sun condition. Specifically, the radiation intensity is the crucial distinction between 1 sun condition and dim lighting. High radiation intensity causes a concomitant increase in the  $R_s/R_{sh}$  value (particularly when the active layer thickness is below 200 nm), which reduces the  $J_{sc}$ , according to Shockley's Equation (7). Conversely, increasing the active layer thickness

decreases the  $R_s/R_{sh}$ , but increases the  $J_{sc}$ . Using a ≥ 280 nm-thick photoactive layer of PPDT2FBT:PC<sub>70</sub>BM, Sang et al. obtained optimum PCE, maximum power,  $J_{sc}$ ,  $V_{oc}$ , and FF of 16%, 44.8 μW cm<sup>-2</sup>, 117 μA cm<sup>-2</sup>, 587 mV, and 65.2%, respectively, under LED lamp (1000 lx). The study also achieved a PCE of 12.5% using an 870 nm-thick active layer.<sup>[29]</sup> These outcomes evidently indicate that the crucial resistance effects on performance of IOPVs devices are dependent on the lighting illumination condition, and the large  $R_{sh}$  related to the thick active layer is critical for the development of efficient IOPVs devices with high  $J_{sc}$  and FF (**Figure 5**). Furthermore, the absorption spectrum of PPDT2FBT is compatible with artificial indoor light sources such as the emission spectral region of LED, which greatly highlights its potential use for indoor applications.<sup>[50]</sup>

In addition, Bae et al. examined the effect of variable active layer thickness of the device subjected to both indoor and outdoor lightings. They discovered that the 210 nm-thick active layer demonstrated the highest PCE, which is attributable to a decrease in series resistance, resulting in an increase of  $J_{sc}$ .<sup>[51]</sup> The effect of active layer thickness on the FF,  $J_{sc}$ , and PCE of the device under 1 sun and LED illumination (1000 lx) is illustrated in **Figure 6**. Young-Jun et al., investigated the effects of different thicknesses of the active layer. They concluded that the PCE of the device that contains the PTB7:PC<sub>71</sub>BM as the active layer with a thickness of 140 nm under indoor light (LED 1000 lx) and 1 sun illumination was 12.3% and 6.1%, respectively. This enhancement is attributable to the rise in  $J_{sc}$ .

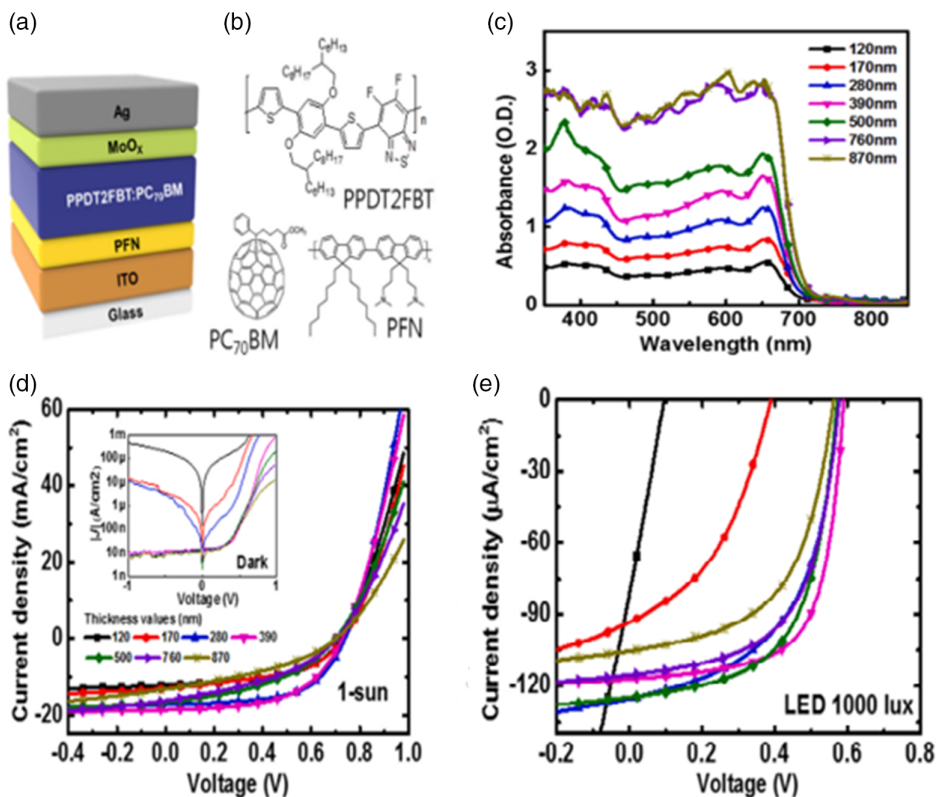


**Figure 5.** a) A device architecture of inverted OPVs. b) Chemical structures of photoactive layer PPDT2FBT:PC<sub>70</sub>BM. c) Absorbance spectral changes with different active layer thickness (120–870 nm) of PPDT2FBT:PC<sub>70</sub>BM. d)  $J$ – $V$  characteristics under 1 sun condition and e) LED (1000 lx) illuminations. Adapted with permission.<sup>[29]</sup> Copyright 2019, Elsevier.

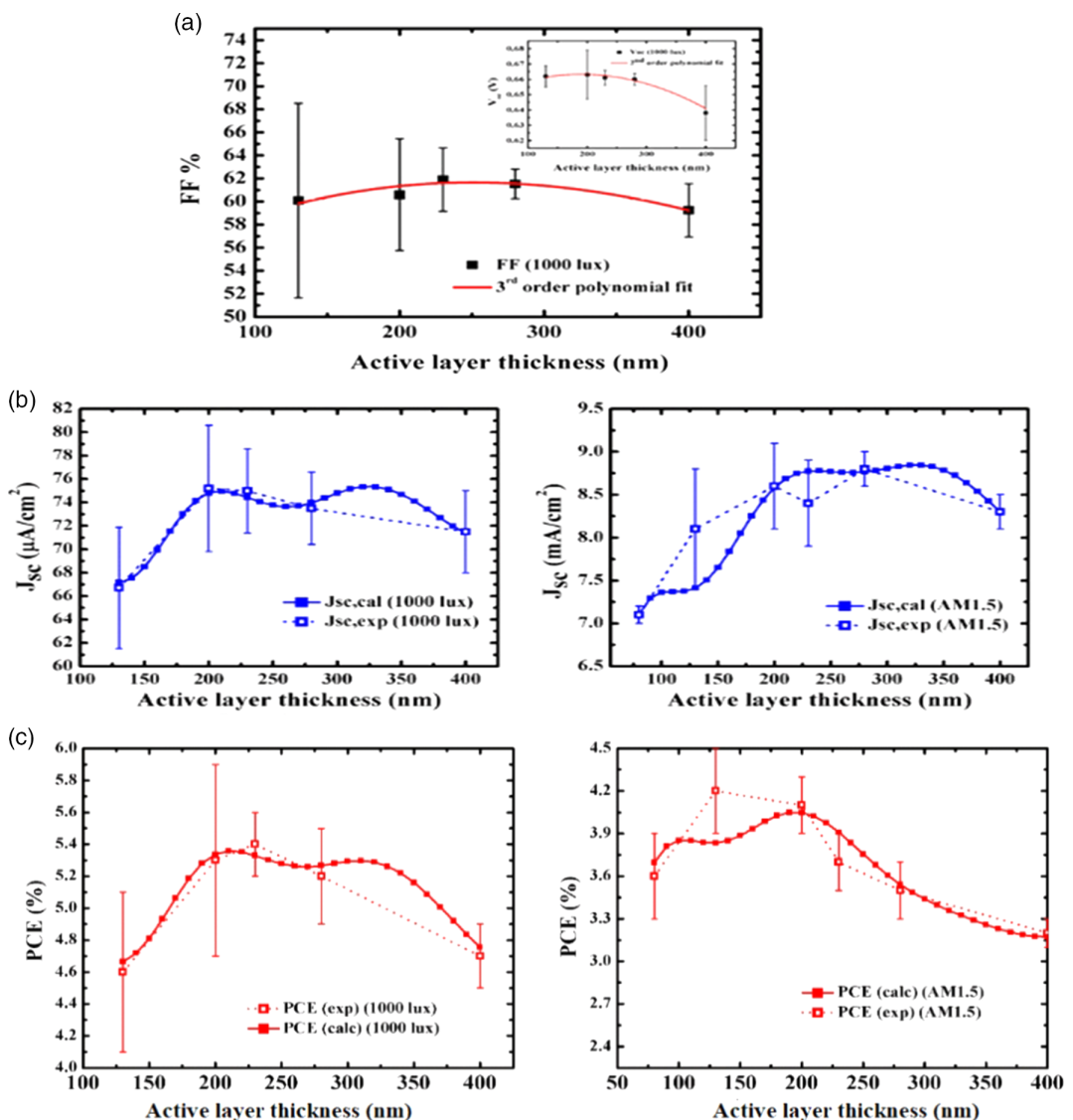


**Figure 6.** a) FF, b)  $J_{sc}$ , and c) PCE for active layer thicknesses from 130 to 400 nm. Adapted with permission.<sup>[51]</sup> Copyright 2019, Elsevier.

under indoor lighting as compared to the  $J_{sc}$  under 1 sun.<sup>[41]</sup> This once more proves that the thickness of the active layer is dependent on the intensity of the incident light, which in turn lowers the  $R_s/R_{sh}$ , and increases the  $J_{sc}$  in accordance with Equation (7). Moreover, a finite-difference time-domain (FDTD)-based simulation was utilized to determine the level of the effective electric field strength generated across a range of photoactive layer thicknesses. The results showed a strong dependence of absorption on the photoactive layer thickness under dim lighting.<sup>[52]</sup> An outline of the electrical parameters of previous reports on the effect of photoactive layer thickness is provided in Table 1.

#### 4. Fullerene as Acceptor-Based OPV Devices

Fullerene derivatives are the most widely used electron acceptors for the fabrication of OPVs due to their relatively high mobility

and high electron affinity.<sup>[54]</sup> Remarkably, the weaker intensities of dim lights than 1 sun illumination prevent photodimerization from arising in fullerene as well as morphological volatility. Regardless of these benefits, the effectiveness of fullerenes is constrained by complex synthesis procedures, relatively preset energy levels, and weak absorption of light in the visible region, resulting in a decline of  $V_{oc}$  when subjected to dim indoor lightings.  $V_{oc}$  is directly proportional to the energy variation between the lowest unoccupied molecular orbital (LUMO) of the acceptor and the highest occupied molecular orbital (HOMO) of the donor. To increase or gain high  $V_{oc}$ , the HOMO of the donor has to be sufficiently deep. However, raising the  $V_{oc}$  value of the OPV devices is a main constraining factor as well as spectral matching for maximization of PCE under indoor condition. For instance, the broad bandgap (which determine the  $V_{oc}$ ) of PDTBTB<sub>z</sub> – 2F<sub>anti</sub> : PC<sub>71</sub>BM polymer produced by Shim et al.<sup>[41]</sup> demonstrated a stronger spectrum matching under

**Table 1.** Summary of electrical parameters to the effects of active layer thickness.

Photoactive layer	Thickness [nm]	Light sources	$J_{sc}$ [ $\mu\text{A cm}^{-2}$ ]	$V_{oc}$ [mV]	FF [%]	PCE [%]	Ref.
PTB7:PC <sub>71</sub> BM	140	1 sun LED 1000 lx	$(13.6 \pm 0.1) \times 10^3$	$670 \pm 9$	$67.4 \pm 0.1$	$6.1 \pm 0.1$	[41]
			$87.6 \pm 3.4$	$569 \pm 3$	$69.3 \pm 4.4$	$12.3 \pm 0.6$	
PPDT2FBT:PC <sub>70</sub> BM	390	1 sun LED 1000 lx	$(16.5 \pm 0.1) \times 10^3$	$717 \pm 3$	$55.2 \pm 1.3$	$6.5 \pm 0.2$	[29]
			$112.3 \pm 1.7$	$586 \pm 3$	$63.5 \pm 1.2$	$14.9 \pm 0.1$	
P3HT:ICBA	200	1 sun LED 1000 lx	$(8.6 \pm 0.5) \times 10^3$	$810 \pm 16$	$58.4 \pm 2.0$	$4.1 \pm 0.2$	[51]
			$75.2 \pm 5.4$	$663 \pm 16$	$60.6 \pm 4.8$	$5.3 \pm 0.6$	
PBDB-TS-4Cl:IT-4F	108	1 sun FL 1000 lx	$21.28 \times 10^3$	850	70.2	12.7	[53]
			129.3	660	74.3	20.7	

indoor lighting (particularly under 1000 lx LED) compared to PTB7, PBDB-T, and P3HT. A power absorption ratio of approximately 96% at 545 nm was achieved using the donor material that consists of PDTBTBz – 2F<sub>anti</sub>. Accordingly, the PDTBTBz – 2F<sub>anti</sub>:PC<sub>71</sub>BM-based device displayed a considerably improved PCE of 23.1% with a  $J_{sc}$ ,  $V_{oc}$ , and FF of  $112.4 \mu\text{A cm}^{-2}$ , 817 mV, and 70.4%, respectively, under indoor LED lighting (500 lx), as evaluated against the binary PTB7:PC<sub>71</sub>BM devices (PCE = 9.11%). Additionally, the study reported that the IOPV prepared with PDTBTBz – 2F<sub>anti</sub>:PC<sub>71</sub>BM exhibited better PCE compared to c-Si PV (PCE of 16.3%). Further on, Lee et al.<sup>[55]</sup> performed experiments to investigate the effect of incorporating WF3F:PC<sub>71</sub>BM into OPVs on  $R_s$ ,  $R_{sh}$ , exciton recombination, and balanced charge transport under indoor LED lighting (500 lx) and 1 sun illumination. The PCE under indoor lighting was enhanced by 83% compared to under 1 sun illumination, which can be attributed to the resulting decline in  $R_s$ . Therefore, in addition to active layer thickness, the light intensity and fullerene type are factors that play crucial roles in the performance of OPV.

Hang et al. used fullerene active layer composite of PCDTBT as donor material and PC<sub>71</sub>BM as an acceptor material. The  $V_{oc}$  reduced from 0.923 V for the 1 sun condition to 0.737 V for the LED tube (300 lx illumination). In contrast, the PCE of the device under 1 sun and indoor light (300 lx illumination) increased from 5.26% to 18.2%, respectively. The optical absorption of this fullerene is the main cause for the enhanced  $J_{sc}$  under various light sources. In contrast, the acceptor layer (PCDTBT) has higher absorption in the 550–650 nm wavelength region. Moreover, the PCDTBT was replaced with another fullerene (P1) to investigate the voltage losses. They concluded that the fullerene P1 managed to reduce voltage losses and to increase the PCE from 5.78% to 19.15% under the 1 sun condition and LED tub (300 lx illumination), respectively. Therefore, reduced energetic defects and improved hole mobilities are the encouraging reasons for utilizing P1.<sup>[56]</sup> Chen et al. utilized an acceptor fullerene ICBA to synthesize BHJ photoactive layer (P3HT:ICBA). The fabricated solar cells achieved the best PCEs of 13.05% and 13.76% under illumination at 500 lx of LED lamp and fluorescent tube, respectively, due to the increase in voltage. Therefore, for indoor applications, the importance of  $V_{oc}$  of OPV devices is the deciding factor in achieving high PCEs. The main reason that led to

enhanced  $V_{oc}$  under dim lighting condition is the high LUMO energy level of the electron acceptor.<sup>[57]</sup> Moreover, OPV device with the photoactive layer BDT-2 T-ID:PNP showed a remarkable increase in PCEs about 16% and  $V_{oc}$  of 0.75 V under LED 200 lx illumination. As the small molecule had deep-lying HOMO energy levels, its performance was three times greater than that of the fullerene (PTB7), resulting in larger  $V_{oc}$  under dim lighting.<sup>[58]</sup> The molecular structures of the fullerene donor and acceptor are shown in Figure 7 and 8, respectively. In addition, Table 2 presents the  $J_{sc}$ ,  $V_{oc}$ , FF, and PCE of some studies related to fullerene-based OPV devices.

## 5. Nonfullerene-Based OPV

The shift from fullerene to nonfullerene acceptors (NFAs) is a crucial transformative approach that enhanced the PCEs of OSCs and IOPVs devices because it enabled the adjustment of energy levels to be compatible with the indoor light spectrum as well as improved the absorption of photons in the visible light region, thus increasing the generation of photocurrent and maximizing the  $V_{oc}$ .<sup>[62–68]</sup> Consequently, nonfullerene (NF)-based OPV devices garnered immense research interest in recent times. Using spin coating method, Yong et al. fabricated a PBDB-TF:IO-4Cl device with an active area of  $1 \text{ cm}^2$ .<sup>[42]</sup> The  $V_{oc}$  was found to surpass 1 V in all the NFA-based devices manufactured, which led to a rise in PCE by  $\approx 26\%$  under LED illumination at 200–1000 lx. The increase in  $V_{oc}$  was attributed to the large gap of NFA named IO-4Cl (3,9-bis[5,6-dichloro-1H-indene-1,3(2H)-dione]-5,5,11,11-tetrakis(4-hexylphenyl)dithieno[2,3-d;2,3-d]-sindaceno[1,2-b:5,6-b']dithiophene, blended with donor material named PBDB-TF (poly[1-(5-(4,8-bis(5-(2-ethylhexyl)-4-fluorothiophen-2-yl)-6-methylbenzo[1,2-b:4,5-b]dithiophen-2-yl)thiophen-2-yl]-5,7-bis(2-ethylhexyl)-3-(5-methylthiophen-2-yl)-4H,8H-benzo[1,2-c:4,5-c]dithiophene-4,8-dione]), which enabled high tolerance or endurance to the dissipation of power in the resistance (i.e., parasitic resistance) under dim lighting. Besides, in 2020, Yan et al. highlighted another approach to increase the  $V_{oc}$  and decrease dissipation of power in the resistance.<sup>[12]</sup> They fabricated a device that comprised the PM6:Y6-O polymer as acceptor and donor materials and PDI-NO as the layer for transporting electrons. The device exhibited an improved PCE of approximately 31% under LED illumination (100–1700 lx), possibly due to the deeper HOMO and better hole-blocking feature of

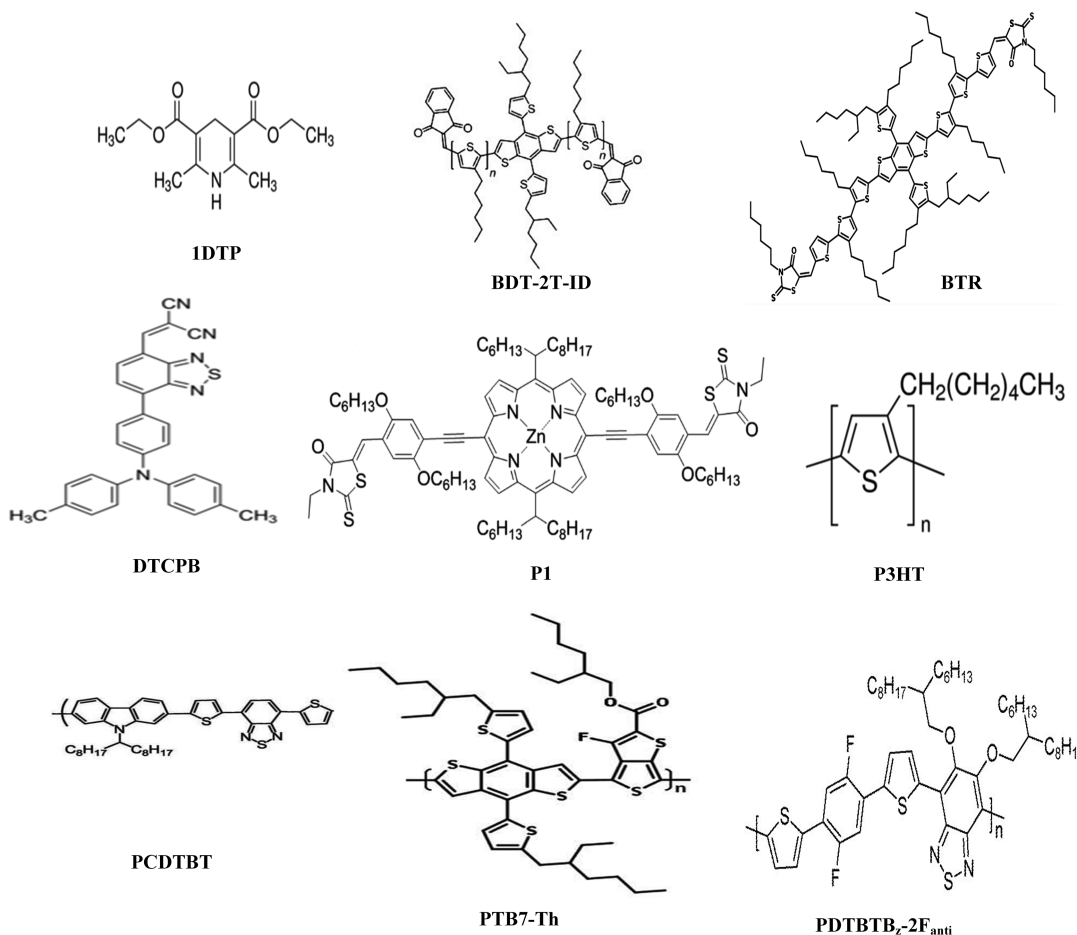


**Figure 7.** Molecular structures of high-performance of fullerene-based OPV donor materials.

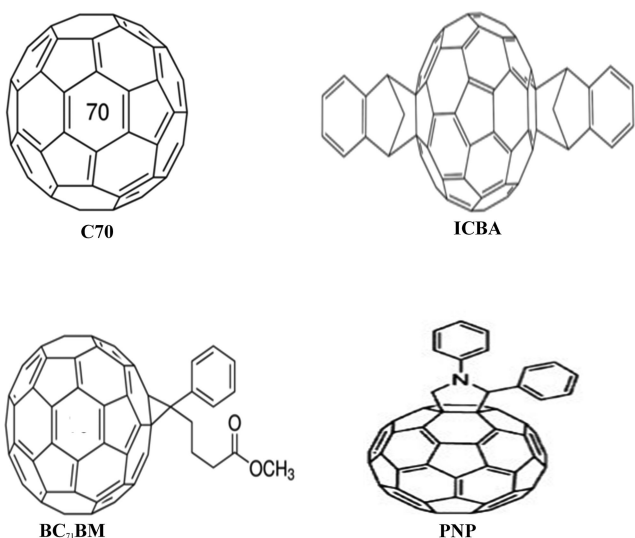


**Figure 8.** Molecular structures of high-performance OPV acceptor materials.

PDI-NO, which decreases the recombination of excitons and minimizes current leakage under dim light settings. This validates the potential use of NFA-based IOPV devices to power IoT electronics much more than fullerene-based IOPVs.

In addition, Yao et al., utilized PBDB-TF:ITCC as photoactive layer-based OPVs due to its high response in the absorption spectrum range of 700–800 nm wavelength. As a result, PCEs of up 20% were achieved under different LED illuminations (200, 500, and 1000 lx) with a photoactive area of 1 cm<sup>2</sup>. The spectrum of the wide-bandgap combination of this polymer is compatible with that of LED illumination, which resulted in minimization of the  $V_{loss}$  in the absorption spectrum range of 700–800 nm wavelength.<sup>[69]</sup> Moreover, the PCE of OPV was enhanced by improving the absorption in the visible light range (400–600 nm) by using PTB7:PC<sub>71</sub>BM:EP-PDI as a photoactive layer due to the crystalline properties of EP-PDI acceptors. PCEs of 15.68% and 8.23% were achieved for IOPV devices under LED illumination (500 lx) and under 1 sun, respectively.<sup>[70]</sup> Furthermore, the IOPV device with the photoactive layer (CD1:PBN-10) displayed  $V_{oc}$  and PCE of 1.16 V and 27%, respectively, under FL 2000 lx. This improved performance is attributed

**Table 2.** Electrical parameters of fullerene-based OPV devices indoor and outdoor applications.

Photoactive layer (D:A)	Light sources	$J_{sc}$ [ $\mu\text{A cm}^{-2}$ ]	$V_{oc}$ [mV]	FF [%]	PCE [%]	Ref.
BTR:PC <sub>71</sub> BM	1 sun FL 1000 lx	$13.3 \times 10^3$	945	75.1	10.5	[22]
		133.1	791	75.2	28.1	
PCDTBT:PC <sub>71</sub> BM	1 sun LED 300 lx	$7.7 \times 10^3$	879	41.5	2.8	[56]
		26.4	698	55.7	13.2	
PC <sub>71</sub> BM P1:	1 sun LED 300 lx	$9.8 \times 10^3$	879	44.9	3.9	[56]
		28.2	755	67.2	18.4	
P3HT:ICBA	1 sun LED 500 lx	$8.2 \times 10^3$	890	67.0	4.9	[57]
		50	730	63.0	13.0	
BDT-2 T-ID:PNP	1 sun LED 200 lx	$13.6 \times 10^3$	940	46.0	5.8	[58]
		24.2	750	68.0	16.0	
DTCPB:C <sub>70</sub>	1 sun FL 800 lx	$11.1 \times 10^3$	900	65.4	6.5	[59]
		79.2	720	64.2	15.7	
PTB7-Th:PC <sub>70</sub> BM	1 sun LED 890 lx	$15.6 \times 10^3$	780	69.0	8.4	[60]
		92.0	620	74.0	11.6	
DTP-ID:PNP	1 sun LED 200 lx	$7.6 \times 10^3$	960	34.0	2.5	[61]
		24.6	670	68.0	19.3	

to the medium energy bandgap (1.93 eV) and alignment of the fitting energy levels of CD1 and PBN-10.<sup>[71]</sup> On the other hand, the stability of organic cells is one of the most important factors that must be considered. The use of NFAs PDI-based OPVs improved the stability of PCE under diverse LED intensities and enhanced  $V_{oc}$ , due to the good compatibility between the absorption and LED emission spectra. Consequently, the PCE decreased from 10.2% to 9% due to LED intensity reduction from 10 000 to 300 lx. For c-Si, the PCE decreased from 10% to 2% at the same range of illumination, which further proves that the c-Si hinders indoor applications because of poor compatibility with the illumination spectrum of the indoor lighting.<sup>[72]</sup> The molecular structures of the fullerene donor and acceptor are shown in Figure 9. The electrical parameters of prior studies on different types of NFA-based IOPV devices are presented in Table 3.

## 6. OPV Devices with Embedded Metallic Nanoparticles

The conversion of light absorption into free-charge carriers is the major difference between the polymer-based and conventional inorganic solar cells. To demonstrate, the light absorption component in common inorganic materials contributes to the generation of holes and free electrons. On the other hand, bound electron–hole pairs (referred to as excitons) are generated in polymer-based materials when there is light absorption. This results in different formation, mobility, and accumulation of charge in OSCs compared to the inorganic equivalent. However, such devices' active layer thickness is restricted to a few 100s of nanometers to compensate for its poor charge mobility of free carriers. This reduced active layer thickness leads to absorption loss because the depth of penetration (i.e., inversely proportional to the absorption coefficient at a specific wavelength) of light

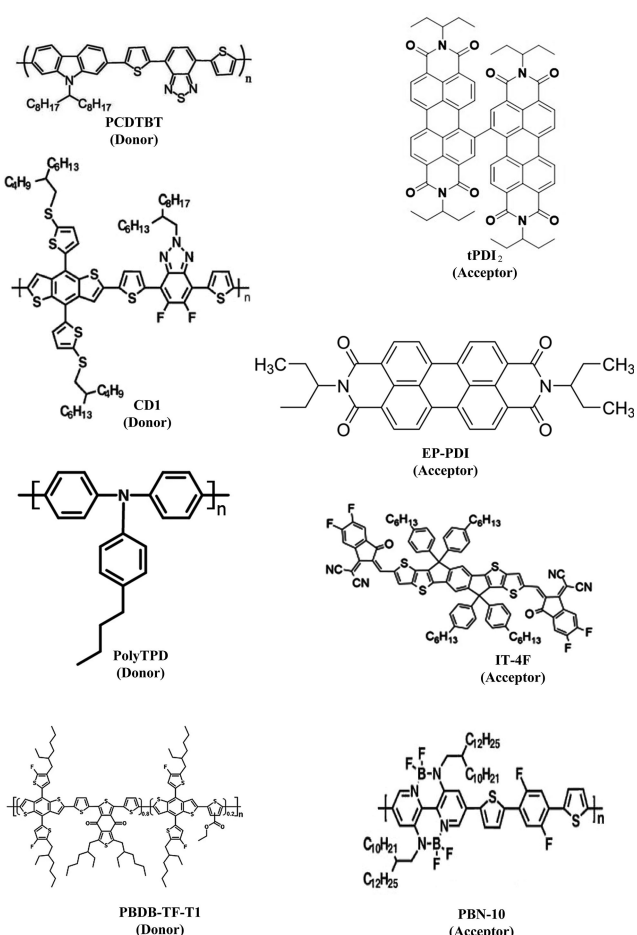


**Figure 9.** Molecular structures of high-performance of NF-based OPV donor and acceptor materials.

**Table 3.** Electrical parameters of NF-based OPV devices indoor and outdoor applications.

Photoactive layer	Light sources	$J_{sc}$ [ $\mu\text{A cm}^{-2}$ ]	$V_{oc}$ [mV]	FF [%]	PCE [%]	Ref.
PCDTBT:PDTSTPD:PC <sub>71</sub> BM	1 sun FL 300 lx	$11.2 \times 10^3$	890	60.2	6.0	[73]
		33.3	730	63.5	20.8	
PBDB-TF:ITCC	1 sun LED 100 lx	$14.5 \times 10^3$	1100	64.3	10.3	[69]
		48.5	949	70.3	20.4	
CD1:PBN-10	1 sun FL 1000 lx	$10.1 \times 10^3$	1290	60.8	7.9	[71]
		120.0	1140	66.2	26.2	
TPD-3 F-51 K:IT-4 F	1 sun FL 1000 lx	$71.2 \times 10^3$	454	62.1	9.8	[74]
		17.6	321	70.6	21.8	
PTB7:PC <sub>71</sub> BM:EP-PDI	1 sun LED 500 lx	$15.3 \times 10^3$	710	55.7	6.3	[70]
		51.0	640	60.9	11.9	
PPDT2FBT:tPDI <sub>2</sub> N-EH	1 sun LED 300 lx	$9.5 \times 10^3$	1020	48.0	4.6	[72]
		20.9	790	49.9	9.0	
J52-F:PM7:BTA3	1 sun LED 300 lx	$12.0 \times 10^3$	1180	61.7	8.7	[75]
		26.5	1000	68.8	20.0	

exceeds the active layer thickness. Here, the use of localized surface plasmon resonance (LSPR) phenomenon is effectual for enhancing the PCE of OSCs (outdoor application under 1 sun condition) and IOPVs, which is attributable to their efficient light scattering and ability to significantly enhance light absorption in the active layer. Additionally, the plasmon resonance of nanoparticles increases the electric field surrounding the MNPs which improves the intrinsic electric field at the boundary separating the donor and acceptor layers that increases the decomposition of excitons. As a result, LSPR effects generated by Au, Ag, and Cu have garnered immense attention from researchers in recent times.<sup>[7,44,76–90]</sup> Nonetheless, it is remarkable that the researchers emphasized the use of MNPs for outdoor photovoltaic applications (OSCs) but disregarded IPV applications in spite of their considerable potential applications (e.g., IoT).

Teng et al. explored the low-power lighting applications of plasmonic-enhanced OPV devices embedded with MNPs.<sup>[91]</sup> The embedded Au NPs, affixed with graphene oxides and poly(ethylene glycol) side chains (Au@PEGGO) in both buffer layer (PEDOT:PSS) and active layer (PBDDTTT-EFT:PC<sub>71</sub>BM), enhanced PCE from 12.3% to 15.6% and  $J_{sc}$  from 0.117 to 0.156 mA/cm<sup>2</sup> under white LED illumination (1000 lx), compared to the device devoid of NPs. Furthermore, the PCEs of the device under illumination from LED and FL lighting exceedingly surpassed the PCE under the 1 sun condition because of the direct effect of LSPR generated by the Au NPs. The improved efficiency suggests that the OPVs embedded with plasmonic MNPs are a potential approach for enhancing the performance of IOPV under dim illumination. In addition, OPVs embedded with copper (Cu) NPs at the cathode interface (i.e., ITO /PEDOT:PSS /PBDDTTT-EFT:PC<sub>71</sub>BM/Ca /Cu NPs/Al) displayed improved PCEs under illuminations from 1 sun, WLED, and FL tube.<sup>[92]</sup> More specifically, the  $V_{oc}$  and PCE of the device increased from 0.77 to 0.79 V and 6.35% to 7.28%, respectively, under 1 sun illumination as compared to the device that is not embedded with Cu NPs. Under FL tube (200 lx) illumination,

the  $V_{oc}$  increased from 0.57 to 0.59 V and PCE improved from 11.30% to 12.65%. Moreover, the enhancement factor of the active layer was increased when measured under WLED illumination. The PCE was optimized at 14.31% under WLED 500 lx. Therefore, the LSPR band of the Cu NPs showed a larger overlap with the spectrum of the WLED, resulting in a more distinct enhancement. In terms of perovskite cells, they exhibited exceptional PCEs under 1 sun and dim light condition. Due to the fact that perovskite photovoltaics have several material advantages, they are often seen as a possible rival to OPVs. In comparison with PCEs for IOPVs, which are typically less than 23%, a substantial proportion of PCEs for perovskite IPVs exceeds 30%.<sup>[24,93–99]</sup>

## 7. Conclusion

Regarding indoor applications, the performance of OPV cells differs from that under 1 sun illumination. This disparity is attributed to variable regions of the spectrum. While solar radiation covers the ultraviolet, visible, and infrared regions, the indoor light sources such as FL tube and LED lamp only emit visible light ranging from 400 to 750 nm. Hence, 700–800 nm of the absorption spectra are redundant in the indoor application of OPV cells or result in  $V_{loss}$ , although OPVs exhibit better stability and higher PCE under indoor light illumination as compared to 1 sun. To further enhance PCE by over 50% for indoor applications, a number of features must be considered. First, to obtain a high  $J_{sc}$ , the donor's bandgap should be narrow enough to absorb the whole incident photons. On the other hand, as the  $V_{oc}$  is directly proportional to the energy difference between the donor's HOMO and acceptor's LUMO energy levels, the donor's bandgap should be wide for a high  $V_{oc}$ . For these reasons, the donor's bandgap should be neither too wide nor too small in order to obtain optimum power output. Additionally, the recombination of trap-mediated charges should be constrained to decrease the  $V_{loss}$ . Second, the active layer or

buffer layer thickness should be increased ( $>200$  nm) via an effective approach to enhance the absorption of the dim lighting. This can be achieved by increasing  $R_{sh}$  through minimizing current leakages. Furthermore, metal nanostructures should be used in the indoor application because of their ability to enhance the electromagnetic field around the metal surface, thus facilitating the accumulation of incident power in LSPR, resulting in increased optical absorption and dissociation of excitons. Given the lack of researches on the behavior of plasmonics under indoor lighting, but exhaustive investigations on the photovoltaic properties under indoor lights, this study recommends two structures that may contribute to boosting the PCE of IOPVs devices: 1) ITO/PEDOT:PSS with Au@Ag NPs (50 nm size)/Y6:BTM (400 nm thickness)/Ca/Al; 2) ITO/PEDOT:PSS with Au@Ag NPs (50 nm size)/PM6:Y6-O (350 nm thickness)/ETL (PDI-NO)/Al electrode. Lastly, this study is positive that advancements in this field will accelerate the fabrication of ideal OPV devices for potential indoor IoT applications.

## Acknowledgements

This research was funded by the Deanship of Scientific Research at Princess Nourah bint Abdulrahman University through the Fast-track Research Funding Program.

## Conflict of Interest

The authors declare no conflict of interest.

## Keywords

indoor organic photovoltaics, IoT, nanoparticles, nonfullerene, PCE, plasmonic, thickness

Received: September 22, 2021

Revised: November 23, 2021

Published online: December 26, 2021

- [1] F. C. Chen, *Adv. Opt. Mater.* **2019**, *7*, 1800662.
- [2] M. Mainville, M. Leclerc, *ACS Energy Lett.* **2020**, *5*, 1186.
- [3] K. Lee, H. D. Um, D. Choi, J. Park, N. Kim, H. Kim, K. Soe, *Cell Rep. Phys. Sci.* **2020**, *1*, 100143.
- [4] S. Dai, X. Zhan, *Adv. Energy Mater.* **2018**, *8*, 1800002.
- [5] R. Søndergaard, M. Hösel, D. Angmo, T. T. Larsen-Olsen, F. C. Krebs, *Mater. Today* **2012**, *15*, 36.
- [6] M. Kaltenbrunner, M. S. White, E. D. Głowacki, T. Sekitani, T. Someya, N. S. Sariciftci, S. Bauer, *Nat. Commun.* **2012**, *3*, 1.
- [7] M. A. Alkhalayfeh, A. A. Aziz, M. Z. Pakhuruddin, *Renewable Sustainable Energy Rev.* **2021**, *141*, 110726.
- [8] S. Kim, M. A. Saeed, S. H. Kim, J. W. Shim, *Appl. Surf. Sci.* **2020**, *527*, 146840.
- [9] S. C. Shin, Y. J. You, J. S. Goo, J. W. Shim, *Appl. Surf. Sci.* **2019**, *495*, 143556.
- [10] J. S. Goo, J. H. Lee, S. C. Shin, J. S. Park, J. W. Shim, *J. Mater. Chem. A* **2018**, *6*, 23464.
- [11] H. S. Ryu, S. Y. Park, T. H. Lee, J. Y. Kim, H. Y. Woo, *Nanoscale* **2020**, *12*, 5792.
- [12] L. K. Ma, Y. Chen, P. C. Chow, G. Zhang, J. Huang, C. Ma, J. Zhang, H. Yin, A. M. H. Cheung, K. S. Wong, S. K. So, H. Yan, *Joule* **2020**, *4*, 1486.
- [13] L. Zhan, S. Li, T. K. Lau, Y. Cui, X. Lu, M. Shi, C.-Z. Li, H. Li, J. Hou, H. Chen, *Energy Environ. Sci.* **2020**, *13*, 635.
- [14] L. Zhu, M. Zhang, G. Zhou, T. Hao, J. Xu, J. Wang, C. Qiu, N. Prine, J. Ali, W. Feng, X. Gu, Z. Ma, Z. Tang, H. Zhu, L. Ying, Y. Zhang, F. Liu, *Adv. Energy Mater.* **2020**, *10*, 1904234.
- [15] C. L. Cutting, M. Bag, D. Venkataraman, *J. Mater. Chem. C* **2016**, *4*, 10367.
- [16] I. Mathews, S. N. Kantareddy, T. Buonassisi, I. M. Peters, *Joule* **2019**, *3*, 1415.
- [17] Y. Bai, C. Zhao, X. Chen, S. Zhang, S. Zhang, T. Hayat, A. Alsaedi, *J. Mater. Chem. A* **2019**, *7*, 15887.
- [18] S. C. Shin, P. Vincent, J. H. Bae, J. J. Lee, M. Nam, D. H. Ko, H. Kim, J. W. Shim, *Dyes Pigm.* **2019**, *163*, 48.
- [19] A. Nardelli, E. Deuschle, L. D. de Azevedo, J. L. N. Pessoa, E. Ghisi, *Renewable Sustainable Energy Rev.* **2017**, *75*, 368.
- [20] Y. Firdaus, V. M. Le Corre, J. I. Khan, Z. Kan, F. Laquai, P. M. Beaujuge, T. D. Anthopoulos, *Adv. Sci.* **2019**, *6*, 1802028.
- [21] M. Freunek, M. Freunek, L. M. Reindl, *IEEE J. Photovoltaics* **2012**, *3*, 59.
- [22] H. K. H. Lee, J. Wu, J. Barbé, S. M. Jain, S. Wood, E. M. Speller, Z. Li, F. A. Castro, J. R. Durrant, W. C. Tsoi, *J. Mater. Chem. A* **2018**, *6*, 5618.
- [23] H. K. Lee, Z. Li, J. R. Durrant, W. C. Tsoi, *Appl. Phys. Lett.* **2016**, *108*, 253301.
- [24] L. K. Jagadamma, S. Wang, *Front. Chem.* **2021**, *9*, 71.
- [25] S. Li, L. Ye, W. Zhao, H. Yan, B. Yang, D. Liu, W. Li, H. Ade, J. Hou, *J. Am. Chem. Soc.* **2018**, *140*, 7159.
- [26] Y. Wang, D. Qian, Y. Cui, H. Zhang, J. Hou, K. Vandewal, T. Kirchartz, F. Gao, *Adv. Energy Mater.* **2018**, *8*, 1801352.
- [27] S. Kim, M. Jahandar, J. H. Jeong, D. C. Lim, *Curr. Altern. Energy* **2019**, *3*, 3.
- [28] N. Yan, C. Zhao, S. You, Y. Zhang, W. Li, *Chin. Chem. Lett.* **2020**, *31*, 643.
- [29] S. C. Shin, C. W. Koh, P. Vincent, J. S. Goo, J. H. Bae, J. J. Lee, C. Shin, H. Kim, H. Y. Woo, J. W. Shim, *Nano Energy* **2019**, *58*, 466.
- [30] L. J. A. Koster, V. D. Mihailescu, R. Ramaker, P. W. Blom, *Appl. Phys. Lett.* **2005**, *86*, 123509.
- [31] C. M. Proctor, C. Kim, D. Neher, T. Q. Nguyen, *Adv. Funct. Mater.* **2013**, *23*, 3584.
- [32] A. Virtuani, E. Lotter, M. Powalla, *Sol. Energy Mater. Sol. Cells* **2006**, *90*, 2141.
- [33] B. Minnaert, P. Veelaert, *Energies* **2014**, *7*, 1500.
- [34] Y. Cui, L. Hong, J. Hou, *ACS Appl. Mater. Interfaces* **2020**, *12*, 38815.
- [35] K. Vandewal, J. Benduhn, V. Nikolis, *Sustainable Energy Fuels* **2018**, *2*, 538.
- [36] C. M. Proctor, T. Q. Nguyen, *Appl. Phys. Lett.* **2015**, *106*, 23-1.
- [37] D. Baran, T. Kirchartz, S. Wheeler, S. Dimitrov, M. Abdelsamie, J. Gorman, R. S. Ashraf, S. Holliday, A. Wadsworth, N. Gasparini, P. Kaienburg, H. Yan, A. Amassian, C. J. Brabec, J. R. Durrant, I. McCulloch, *Energy Environ. Sci.* **2016**, *9*, 3783.
- [38] X. Xu, T. Yu, Z. Bi, W. Ma, Y. Li, Q. Peng, *Adv. Mater.* **2018**, *30*, 1703973.
- [39] V. Gupta, A. K. K. Kyaw, D. H. Wang, S. Chand, G. C. Bazan, A. J. Heeger, *Sci. Rep.* **2013**, *3*, 1.
- [40] T. Fukuhara, Y. Tamai, H. Ohkita, *Sustainable Energy Fuels* **2020**, *4*, 4321.
- [41] Y. J. You, C. E. Song, Q. V. Hoang, Y. Kang, J. S. Goo, D. H. Ko, J.-J. Lee, W. S. Shin, J. W. Shim, *Adv. Funct. Mater.* **2019**, *29*, 1901171.
- [42] Y. Cui, Y. Wang, J. Bergqvist, H. Yao, Y. Xu, B. Gao, C. Yang, S. Zhang, O. Inganäs, F. Gao, J. Hou, *Nat. Energy* **2019**, *4*, 768.
- [43] Y. Zhou, T. M. Khan, J. W. Shim, A. Dindar, C. Fuentes-Hernandez, B. Kippelen, *J. Mater. Chem. A* **2014**, *2*, 3492.

- [44] M. A. Alkhalayfeh, A. A. Aziz, M. Z. Pakhuruddin, *Solar Energy* **2021**, 214, 565.
- [45] C. P. Chen, I. C. Lee, Y. Y. Tsai, C. L. Huang, Y. C. Chen, G. W. Huang, *Org. Electron.* **2018**, 62, 95.
- [46] Q. Fan, R. Ma, T. Liu, W. Su, W. Peng, M. Zhang, Z. Wang, X. Wen, Z. Cong, Z. Luo, L. Hou, F. Liu, W. Zhu, D. Yu, H. Yan, E. Wang, *Solar RRL* **2020**, 4, 2000142.
- [47] J. Yuan, Y. Zhang, L. Zhou, G. Zhang, H. L. Yip, T. K. Lau, X. Lu, C. Zhu, H. Peng, P. A. Johnson, M. Leclerc, Y. Cao, J. Ulanski, Y. Li, Y. Zou, *Joule* **2019**, 3, 1140.
- [48] Y. Lin, B. Adilbekova, Y. Firdaus, E. Yengel, H. Faber, M. Sajjad, X. Zheng, E. Yarali, A. Seitkhan, O. M. Bakr, A. El-Labban, U. Schwingenschlögl, V. Tung, I. McCulloch, F. Laquai, T. D. Anthopoulos, *Adv. Mater.* **2019**, 31, 1902965.
- [49] K. Li, Y. Wu, Y. Tang, M. A. Pan, W. Ma, H. Fu, C. Zhan, J. Yao, *Adv. Energy Mater.* **2019**, 9, 1901728.
- [50] H. Kang, M. A. Uddin, C. Lee, K. H. Kim, T. L. Nguyen, W. Lee, Y. Li, C. Wang, H. Y. Woo, B. J. Kim, *J. Am. Chem. Soc.* **2015**, 137, 2359.
- [51] P. Vincent, S. C. Shin, J. S. Goo, Y. J. You, B. Cho, S. Lee, D.-W. Lee, S. R. Kwon, K.-B. Chung, J.-J. Lee, J.-H. Bae, J. W. Shim, H. Kim, *Dyes Pigm.* **2018**, 159, 306.
- [52] P. Vincent, J. W. Shim, J. Jang, I. M. Kang, P. Lang, J. H. Bae, H. Kim, *Energies* **2019**, 12, 1838.
- [53] H. I. Je, E. Y. Shin, K. J. Lee, H. Ahn, S. Park, S. H. Im, Y.-H. Kim, H. J. Son, S.-K. Kwon, *ACS Appl. Mater. Interfaces* **2020**, 12, 23181.
- [54] N. Bauer, Q. Zhang, J. Zhao, L. Ye, J. H. Kim, I. Constantinou, L. Yan, F. So, H. Ade, H. Yan, W. You, *J. Mater. Chem. A* **2017**, 5, 4886.
- [55] R. Singh, C. L. Chochos, V. G. Gregoriou, A. D. Nega, M. Kim, M. Kumar, S.-C. Shin, S. H. Kim, J. W. Shim, J.-J. Lee, *ACS Appl. Mater. Interfaces* **2019**, 11, 36905.
- [56] H. Yin, S. Chen, S. H. Cheung, H. W. Li, Y. Xie, S. W. Tsang, X. Zhu, S. So, *J. Mater. Chem. C* **2018**, 6, 9111.
- [57] S. S. Yang, Z. C. Hsieh, M. L. Keshtov, G. D. Sharma, F. C. Chen, *Solar RRL* **2017**, 1, 1700174.
- [58] R. Arai, S. Furukawa, Y. Hidaka, H. Komiyama, T. Yasuda, *ACS Appl. Mater. Interfaces* **2019**, 11, 9259.
- [59] C. H. Chen, H. C. Ting, Y. Z. Li, Y. C. Lo, P. H. Sher, J. K. Wang, T.-L. Chiu, C.-F. Lin, I.-S. Hsu, J.-H. Lee, S.-W. Liu, K.-T. Wong, *ACS Appl. Mater. Interfaces* **2019**, 11, 8337.
- [60] S. Mori, T. Gotanda, Y. Nakano, M. Saito, K. Todori, M. Hosoya, *Jpn. J. Appl. Phys.* **2015**, 54, 071602.
- [61] R. Arai, S. Furukawa, N. Sato, T. Yasuda, *J. Mater. Chem. A* **2019**, 7, 20187.
- [62] K. Cnops, G. Zango, J. Genoe, P. Heremans, M. V. Martinez-Diaz, T. Torres, D. Cheyns, *J. Am. Chem. Soc.* **2015**, 137, 8991.
- [63] B. Kan, J. Zhang, F. Liu, X. Wan, C. Li, X. Ke, Y. Wang, H. Feng, Y. Zhang, G. Long, R., H. Friend, A. A. Bakulin, Y. Chen, *Adv. Mater.* **2018**, 30, 1704904.
- [64] H. Li, Y. J. Hwang, B. A. Courtright, F. N. Eberle, S. Subramaniyan, S. A. Jenekhe, *Adv. Mater.* **2015**, 27, 3266.
- [65] Z. Luo, H. Bin, T. Liu, Z. G. Zhang, Y. Yang, C. Zhong, B. Qiu, G. Li, W. Gao, D. Xie, K. Wu, Y. Sun, F. Liu, Y. Li, C. Yang, *Adv. Mater.* **2018**, 30, 1706124.
- [66] H. Sun, X. Song, J. Xie, P. Sun, P. Gu, C. Liu, F. Chen, Q. Zhang, Z.-K. Chen, W. Huang, *ACS Appl. Mater. Interfaces* **2017**, 9, 29924.
- [67] J. Zhang, K. Jiang, G. Yang, T. Ma, J. Liu, Z. Li, J. Y. L. Lai, W. Ma, H. Yan, *Adv. Energy Mater.* **2017**, 7, 1602119.
- [68] Z. Zheng, O. M. Awartani, B. Gautam, D. Liu, Y. Qin, W. Li, A. Bataller, K. Gundogdu, H. Ade, J. Hou, *Adv. Mater.* **2017**, 29, 1604241.
- [69] Y. Cui, H. Yao, T. Zhang, L. Hong, B. Gao, K. Xian, J. Qin, J. Hou, *Adv. Mater.* **2019**, 31, 1904512.
- [70] R. Singh, S. C. Shin, H. Lee, M. Kim, J. W. Shim, K. Cho, J.-J. Lee, *Chem.—Eur. J.* **2019**, 25, 6154.
- [71] Z. Ding, R. Zhao, Y. Yu, J. Liu, *J. Mater. Chem. A* **2019**, 7, 26533.
- [72] S. V. Dayneko, M. Pahlevani, G. C. Welch, *ACS Appl. Mater. Interfaces* **2019**, 11, 46017.
- [73] H. Yin, J. K. W. Ho, S. H. Cheung, R. J. Yan, K. L. Chiu, X. Hao, S. K. So, *J. Mater. Chem. A* **2018**, 6, 8579.
- [74] C. Y. Liao, Y. Chen, C. C. Lee, G. Wang, N. W. Teng, C. H. Lee, W.-L. Li, Y.-K. Chen, C.-H. Li, H.-L. Ho, P. H.-S. Tan, B. Wang, Y.-C. Huang, R. M. Young, M. R. Wasielewski, T. J. Marks, Y.-M. Chang, A. Facchetti, *Joule* **2020**, 4, 189.
- [75] Y. Bai, R. Yu, Y. Bai, E. Zhou, T. Hayat, A. Alsaedi, Z. Tan, *Green Energy Environ.* **2021**, 6, 920.
- [76] M. A. Alkhalayfeh, A. A. Aziz, M. Z. Pakhuruddin, K. M. M. Katubi, *Phys. Status Solidi A* **2021**, 218, 2100310.
- [77] M. A. Alkhalayfeh, A. Abdul Aziz, M. Z. Pakhuruddin, *Materials* **2021**, 14, 5591.
- [78] M. Mohan, R. Sekar, M. A. Namboothiry, *RSC Adv.* **2020**, 10, 26126.
- [79] A. T. Nair, C. Anoop, G. A. Vinod, V. Reddy, *Org. Electron.* **2020**, 86, 105872.
- [80] Q. N. Tran, H. K. Lee, J. H. Kim, S. J. Park, *J. Nanosci. Nanotechnol.* **2020**, 20, 304.
- [81] S. Koul, *Trans. Electr. Electron. Mater.* **2020**, 21, 293.
- [82] B. Rezaei, F. Afshar-Taromi, Z. Ahmadi, S. A. Rigi, N. Yousefi, *Mater. Chem. Phys.* **2019**, 228, 325.
- [83] N. Ahmadi, *J. Nanophotonics* **2021**, 15, 036010.
- [84] H. Gao, J. Meng, J. Sun, J. Deng, *J. Mater. Sci.: Mater. Electron.* **2020**, 31, 10760.
- [85] A. Ali, D. Said, M. Khayyat, M. Boustimi, R. Seoudi, *Res. Phys.* **2020**, 16, 102819.
- [86] J. Shin, M. Song, H. Hafeez, P. J. Jeusraj, D. H. Kim, J. C. Lee, W. H. Lee, D. K. Choi, C. H. Kim, T.-S. Bae, S. M. Yu, K.-H. Kim, H.-G. Park, K.-B. Chung, A. Song, Y.-C. Kang, J. Park, C. S. Kim, S. Y. Ryu, *Org. Electron.* **2019**, 66, 94.
- [87] Z. Babaei, B. Rezaei, M. K. Pisheh, F. Afshar-Taromi, *Mater. Chem. Phys.* **2020**, 248, 122879.
- [88] H. Kaçuş, Ş Aydoğan, M. Biber, Ö Metin, M. Sevim, *Mater. Res. Express* **2019**, 6, 095104.
- [89] D. Said, A. Ali, M. Khayyat, M. Boustimi, M. Loulou, R. Seoudi, *Heliyon* **2019**, 5, e02675.
- [90] X. Li, Y. Cao, S. Li, W. Li, Z. Bo, *Mater. Lett.* **2020**, 268, 127599.
- [91] N. W. Teng, S. S. Yang, F. C. Chen, *IEEE J. Photovoltaics* **2018**, 8, 752.
- [92] C. L. Huang, G. Kumar, G. D. Sharma, F. C. Chen, *Appl. Phys. Lett.* **2020**, 116, 253302.
- [93] K. L. Wang, Y. H. Zhou, Y. H. Lou, Z. K. Wang, *Chem. Sci.* **2021**, 12, 11936.
- [94] M. Li, C. Zhao, Z. K. Wang, C. C. Zhang, H. K. Lee, A. Pockett, J. Barbé, W. C. Tsoi, Y.-G. Yang, M. J. Carnie, X.-Y. Gao, W.-X. Yang, J. R. Durrant, L.-S. Liao, S. M. Jain, *Adv. Energy Mater.* **2018**, 8, 1801509.
- [95] S. Castro-Hermosa, G. Lucarelli, M. Top, M. Fahland, J. Fahleich, T. M. Brown, *Cell Rep. Phys. Sci.* **2020**, 1, 100045.
- [96] M. Lee, E. Choi, A. M. Soufiani, J. Lim, M. Kim, D. Chen, M. A. Green, J. Seidel, S. Lim, J. Kim, X. Dai, R. Lee-Chin, B. Zheng, Z. Hameiri, J. Park, X. Hao, J. S. Yun, *Adv. Funct. Mater.* **2021**, 31, 2008908.
- [97] J. Xu, J. Xi, H. Dong, N. Ahn, Z. Zhu, J. Chen, P. Li, X. Zhu, J. Dai, Z. Hu, B. Jiao, X. Hou, J. Li, Z. Wu, *Nano Energy* **2021**, 88, 106286.
- [98] C. H. Chen, Y. H. Lou, K. L. Wang, Z. H. Su, C. Dong, J. Chen, Y.-R. Shi, X.-Y. Gao, Z.-K. Wang, *Adv. Energy Mater.* **2021**, 11, 2101538.
- [99] A. Venkateswararao, J. K. Ho, S. K. So, S. W. Liu, K. T. Wong, *Mater. Sci. Eng.: R: Rep.* **2020**, 139, 100517.



**Muheeb Ahmad Alkahalayfeh** is currently a Ph.D. student under the supervision of Prof. Azlan Abdul Aziz and Dr. Mohd Zamir Pakhuruddin at Universiti Sains Malaysia. He got his B.Sc. degree in physics from Al-Hussein Bin Talal University in 2011, followed by an M.Sc. degree in physics from Mu'tah University, Jordan. His research interests mainly focus on enhanced polymer and perovskite solar cells with embedded plasmonic nanoparticles.



**Azlan Abdul Aziz** obtained his M.Sc. and Ph.D. degrees from the University of Manchester Institute of Science and Technology (UMIST), UK, in 1994 and 1999, respectively. His research interest is primarily on sensors for electronics and health applications. He is now a professor in nanomaterials and nanostructures at the School of Physics, Universiti Sains Malaysia (USM), and he is currently one of the lead researchers at Makmal Nano (NanoLAB) at the School of Physics and the principal researcher with the Nano Biotechnology Research and Innovation (NanoBRI@INFORMM) team at the Institute for Research in Molecular Medicine (INFORMM) in USM.



**Mohd Zamir Pakhuruddin** is a senior lecturer at the School of Physics, Universiti Sains Malaysia, Malaysia. In 2016, he obtained his Ph.D. degree in photovoltaics engineering from the University of New South Wales, Australia. Before joining academia, he was in the semiconductor industry with SilTerra and Fuji Electric, as a photolithography and sputtering research and development engineer, respectively. His current research is on photovoltaic materials and devices, focusing on black silicon and perovskite solar cells.

**Khadijah Mohammedsaleh M. Katubi** received her Ph.D. degree in chemistry from the University of Hull, UK (2010–2012). Currently, she is an assistant professor in the Chemistry Department, College of Science, Princess Nourah bint Abdulrahman University, Riyadh, Saudi Arabia. Her research interests are focused on nanomaterials for environmental applications, synthesis, and characterization of polymers with inorganic nanostructured compounds, and nanostructured stable perovskite and polymer solar cells.



**Neda Ahmadi** is an assistant professor at Azad University in Iran. She received her Ph.D. degree in condensed matter physics at Plasma Physics Research Center, Science and Research Branch, Iran, in 2015. She spent 11 months at Australian National University as a campus visitor in 2016. She is currently working on organic and perovskite materials and light management techniques for the efficiency enhancement of solar cells.